Desalination and Water Treatment
www.deswater.com

doi: 10.5004/dwt.2017.20160

75 (2017) 174–182
May

Effect of calcination temperature of sawdust as a sorbent for bromo phenol red removal from aqueous solutions

Akram Alikarimi, Saeedeh Hashemian*, Masumeh Tabatabaee

Chemistry Department, Islamic Azad University, Yazd Branch, Yazd, Iran, Tel. +98 3187275 2; Fax: +98 3537266065; emails: Sa_hashemian@iauyazd.ac.ir (S. Hashemian), a.karimi0055@gmail.com (A. Alikarimi), tabatabaee@iauyazd.ac.ir (M. Tabatabaee)

Received 19 April 2016; Accepted 11 August 2016

ABSTRACT

Sawdust (SD) was calcinated at different temperatures (100°C–1,000°C). SDs were characterized by FTIR and SEM. SEM image showed spherical and uniformed shapes with particle sizes of 50 and 35 nm for SD calcinated at 600°C and 1,000°C, respectively. The adsorption of bromophenol red (BPR) by SDs was studied. The optimum conditions for the maximum removal of BPR were found at pH > 6, contact time 60 min and adsorbent dose of 0.1 g. The sequence capabilities of SD calcinated at different temperatures for adsorption of BPR were as follows: $SD_{1,000} > SD_{800} > SD_{600} > SD_{400} > SD_{200} > SD_{100}$. Two common kinetic models, Lagergren's pseudo-first-order and pseudo-second-order models were employed to describe the adsorption kinetics. Adsorption of BPR was followed by pseudo-second-order kinetic model. Equilibrium data were analyzed by Freundlich and Langmuir isotherms. The best fit to the data for adsorption of BPR was obtained with the Langmuir isotherm. Thermodynamic results showed the endothermic and spontaneous process. The spent SD was regenerated through simple physical method.

Keywords: Adsorption; Bromo phenol red; Calcination; Sawdust

1. Introduction

Colored wastewater generally comes from dyes or pigments manufacturing, textile industries, pulp and paper mills and laboratories. The disposal of dyes into water systems destructs the esthetic nature and poses a serious threat to human health and affects the food cycle in water ecosystems. Due to their chemical structures, in which they usually contain complex aromatic textures, dyes are toxic, carcinogenic and resistant to fading on exposure to light, heat, water, microbes and many chemicals [1]. Bromophenol red is a hazardous dye and is most commonly used for dyeing cotton, silk, paper, leather. It is also used in manufacturing of paints and printing inks. Various physical, chemical and biological treatment techniques were employed for removing dyes from wastewater. Many synthetic dyes do not easily decompose in biological treatments due to their toxic effects on microorganisms. Among the various available physical and chemical processes, adsorption technology is considered to be one of the most effective and proven technology for decolorization in water and effluent [2]. Adsorbents have high affinity toward organic compounds [3–5]. Low costs, simple preparation and high adsorption capacity are a few of many added values desired for the adsorbents.

Adsorption on activated carbon has been proven to be very effective in removing dyes from aqueous solutions. However, activated carbon is still considered expensive; so, the research is, currently, focused on the development of low-cost adsorbents for this purpose. Because of its relatively high cost, attempts have been made to utilize low cost, naturally occurring sorbents to remove trace contaminants from wastewater [6–8].

Such sorbents are attractive because of their abundant availability at low or no cost and their good performance in removing dyes from aqueous solutions. In recent years, there has been growing attention in finding low-cost materials and

* Corresponding author.

effective adsorbents such as different carbon-based materials [9–13]. Low-cost adsorbents including natural agricultural and industrial by-product wastes are also attractive and interesting for removing dyes [14–16]. Sorbents such as tea waste [17], rice straw [18], palm ash [19], biomass fly ash [20], chitosan/oil palm ash [21], pomelo [22], oil palm trunk fiber [23], dried biomass of Baker's yeast [24] and rattan sawdust [25] have also been considered for dye removal from aqueous solutions. Removal of different dyes by adsorption onto ZnO, ZnS, Ag and Ru nanoparticles loaded on activated carbon has been investigated [26–32].

Carbon materials fabricated from waste biomass have shown promising applications as sorption. Among agricultural waste materials, sawdust is one of the promising adsorbents for removing dye pollutants from wastewaters. Studies have shown that sawdust and modified sawdust have a sorption capacity for the removal of most kinds of dyes from aqueous solutions. If sawdust is used as a sorbent, it will benefit the environment in terms of solid waste management [30–35].Therefore, sawdust has proven to be a promising effective material for removal of dyes from wastewaters.

Sawdust consists of cellulose, lignin and hemicelluloses. Cellulose is composed of a long chain of glucose molecules. Lignin is a complex polymer composed of phenylpropane units, and hemicelluloses are branched polymers composed of xylose, arabinose, galactose, mannose, and glucose. Hemicelluloses bind the bundles of cellulose fibrils to form microfibrils; also, they cross-link with lignin, creating a complex web of bonds which enhance the stability of the cell walls and structural strength [11–14]. The lignocellulosic material of sawdust includes a wide variety of hydroxyl groups which can be used as active sites for the preparation of solid acid catalysts.

The objective of the present study is to investigate possibility of inexpensive forestry waste sawdust and calcinated sawdust (SD) for removal of bromophenol red (BPR) from aqueous solutions. The optimum conditions were investigated at different pH, contact time and sorbent concentration. The kinetics, isotherm and thermodynamic of adsorption process were determined.

2. Experimental

2.1. Materials and methods

All chemicals used were of analytical grade purity and were used as received without any purification. All of the chemicals were purchased from Merck Chemical Co. (Germany). Distillated water was used in all the experiments.

Bromophenol Red (3′, 3″-dibromophenolsulfonphthalein), CAS number 2800-80-8 with chemical formula of $C_{19}H_{12}Br_2O_5S$ (BPR) as a sample of pollutant was used. It has molecular weight of 512.17 g mol^{-1} (Fig. 1). The standard solution of BPR 1,000 mg L^{-1} was prepared and diluted subsequently whenever necessary.

The sawdust (walnut tree in Yazd) was collected from sawmill wood market in Iran. The collected samples were washed repeatedly with deionized water to remove extraneous materials and salts. The sorbent was, then, dried in furnace at 100°C–1,200°C for 6 h, and sieved. The sieved mass fraction between 250 and 350 mm was used for the sorption study.

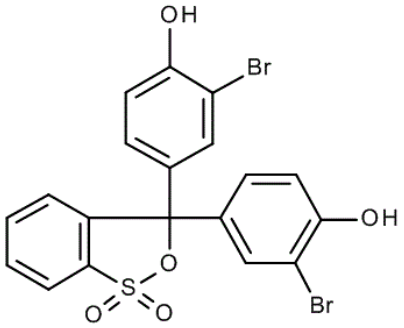

Fig. 1. Chemical structure of BPR.

All pH measurements were carried out with an ISTEK- 720P pH meter. UV-Vis spectrophotometer 160-A Shimadzu was used for determination of concentration of BPR. IR measurements were performed by FTIR tensor-27 of Burker Co., using the KBr pellet between the ranges of 500–4,000 cm^{-1}. The powder X–ray diffraction studies were made on a Philips PW1840 diffractometer using Ni-filtered Cu k_α radiation. The average particle size and morphology of samples were observed by SEM using a Hitachi S-3500 scanning electron microscope.

All experiments were conducted at 25°C. 0.1 g of sorbent was added in 50 ml dye sample on rotary shaker at a constant speed of 300 rpm. After different contact times (0–180 min), the sorbent was removed from the solution and the equilibrium concentration of BPR dye in the solution was determined with UV spectrophotometer at the wavelength of 437 nm (λ_{max}). To optimize the sorbent dosage, different amounts of the sorbents were examined. A known amount of sorbent (0.01–0.1 g) was added to 50 mL of dye solutions. To study the effect of solution pH, 0.10 g of SD was agitated with 50 mL of dye solution of 10 mg L^{-1} using water-bath shaker at 25°C. The experiment was conducted at different pH value ranging from 2 to 12. At equilibrium, the dye concentrations were measured by a double beam UV/vis Spectrophotometer (Shimadzu Model UV 160-A, Japan) at 437 nm. The pH was adjusted by adding a few drops of diluted 0.1 N NaOH or 0.1 N HCl. Each experiment was repeated five times, and the average results were given. Relative standard deviation (% RSD) was determined between 1.95% and 2.85% for each points at all the experiments.

The amount of equilibrium adsorption, q_e (mg g^{-1}), was calculated by:

$$q_e = (C_0 - C_e)V/W \quad (1)$$

where C_0 and C_e (mg/L) are the liquid-phase concentrations of dye at initial and equilibrium, respectively. V (L) is the volume of the solution and W (g) is the mass of dried sorbent used.

3. Results and discussion

3.1. Characterization

Since the sorption is a surface phenomenon, the rate and degree of sorption is highly dependent on the surface functional groups, pore sizes and surface area of the sorbent.

Therefore, SEM is known as one of the most widely used surface diagnostic tools. The SEM images of SD calcinated at different temperatures (100°C, 400°C, 600°C and 1,000°C) are shown in Fig. 2. The SEM micrographs show that the SD has a fibrous structure and rough surface morphology with some pores. From the SEM analysis, it was found that there were holes and cave type openings on the surface of the adsorbent which would have more surface area available for adsorption. Increasing the calcination temperature of SD caused the smaller and more uniformed spherical shape of SD.

The SD calcinated at 100°C, 400°C, 600°C and 1,000°C had particle sizes of 10 um, 100, 50 and 35 nm, respectively.

The results of energy-dispersive X-ray spectroscopy (EDX) were recorded to investigate the elemental composition of SDs. The results demonstrated that mainly C and O appeared in SD samples. After calcination of SDs, some of impurities were lost and the main compound of SD was C.

The X-ray diffraction (XRD) technique is a powerful tool to analyze the crystalline nature of the materials. The X-ray diffraction patterns of SD_{100} and $SD_{1,000}$ were examined. The diffractions are shown in Fig. 3 and show two diffraction peaks; a peak appears at 24° and another one at 45°. The positions of the peaks due to d_{100} and d_{002} reflections are attributed to $2\theta = 24°$ and 45°, respectively. The sharp diffraction of 45° is similar to activated carbon (Merck) [36].

The apparent crystallite size (L) was estimated with the use of the Scherrer Equation:

$$L = K \lambda / \beta \cos \theta \quad (2)$$

where K is a constant with a value of 0.94, λ is the X-ray wavelength (0.1542 nm), β is the width of the diffraction peak at half of the intensity, and θ is the Bragg angle corresponding to the (002) plane. The particle size of $SD_{1,000}$ was determined by Scherrer equation (32–40 nm).

The FTIR is generally used to identify some of the characteristic functional groups capable of interaction with sorbate. Fig. 4 shows the FTIR spectra of SDs. The broad band 3,200–3,600 cm^{-1} indicates the presence of both free and hydrogen bonded OH groups on the SD surface. The band around 1,400 is attributed to CH_3 bending vibration and some interactions between SD stretching and in plane C–O–H and C–H bending. The other characteristic of peaks at 3,441 cm^{-1} and 1,632 cm^{-1} are due to O–H stretching and O–H bending, respectively. The band at 1,437 cm^{-1} is due to aromatic ring of lignin of SD (Fig. 4(a)) which disappears at SD calcinated at

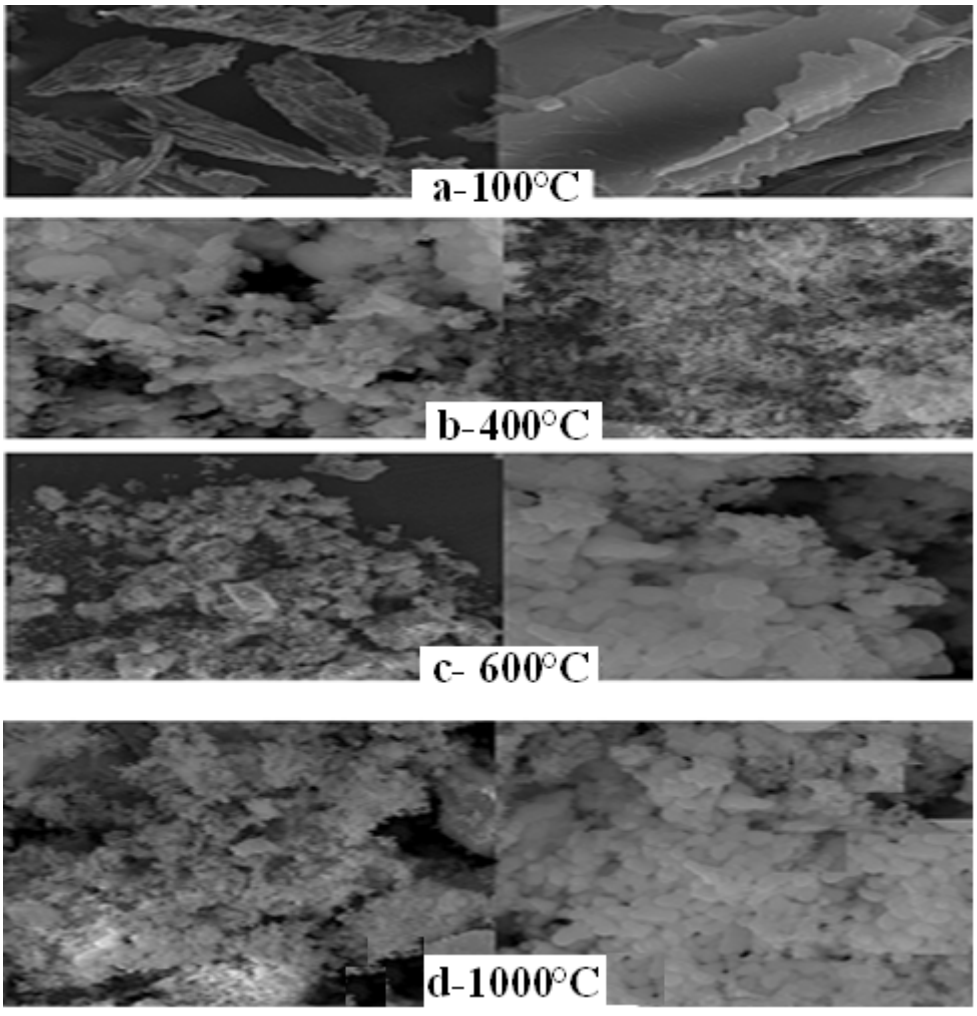

Fig. 2. SEM image sawdust cacinated at (a)-100°C, (b)-400°C, (c)-600°C and (d)-1,000°C.

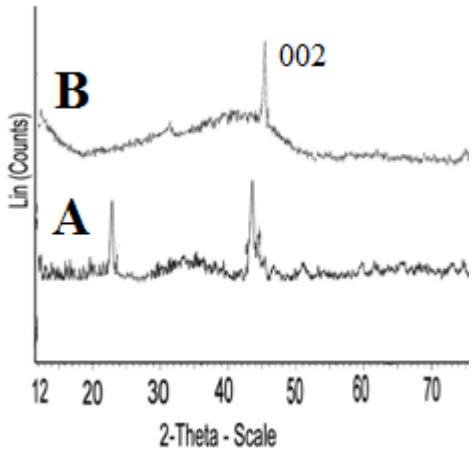

Fig. 3. XRD patterns of (A) SD_{100}, (B) $SD_{1,000}$.

1,000°C (Fig. 4(f)) [23]. The results of FTIR show the calcination of SD cause disappearance of some bonds and weakening of the other ones compared to local sawdust.

The specific surface area (BET method) of SD_{100}–$SD_{1,000}$ were determined. The specific surface area of SD_{100}, SD_{600} and $SD_{1,000}$ were 220, 843 and 1,050 $m^2 g^{-1}$, respectively. Calcination of SD increased the surface area; therefore, the contact time of dye with SD decreased. The BET surface area of $SD_{1,000}$ was similar to activated carbon [36].

3.2. Study of adsorption

The treatment way for BPR is a crucial factor for achievement of the highest adsorption capacity and reducing the cost of sample preparation. Therefore, the effect of different parameters on adsorption process was investigated.

3.2.1. Effect of contact time

Contact time is one of the important factors affecting on batch adsorption process; therefore, different contact times (0–180 min) were studied for removal of BPR dye. The effect of contact time on the removal of BPR using SD for 0.1 g SD and 50 mL of BPR 10 mg L^{-1} is shown in Fig. 5. It is obvious that increasing the contact time improved the adsorption process. The adsorption process increased sharply at the initial stage indicating the availability of readily accessible sites. The results indicated very quick rate of adsorption of BPR in the initial 15 min and thereafter, the adsorption rate declined gradually and reached the equilibrium at about 30 min. The higher adsorption rate at the initial stage may be due to availability of more number of vacant sites. As a result, there exists increased BPR concentration gradient in solution and on the SD surface. After a certain period of time, this gradient is reduced due to accumulation of BPR dye in the vacant sites, leading to a decrease in adsorption rate.

The time required to attain the equilibrium for SD calcinated at different temperatures was different. It is obvious that the SD calcinated at 1,000°C had the highest adsorption efficiency of BPR due to high surface area. The sequence capability of SD calcinated at different temperatures for adsorption of BPR was as follows: $SD_{1,000} > SD_{800} > SD_{600} > SD_{400} > SD_{200} > SD_{100}$.

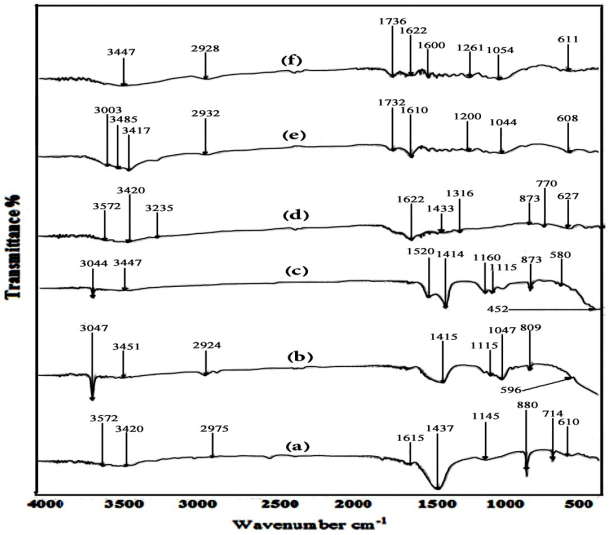

Fig. 4. FTIR of SD cacinated at (a) 100°C, (b) 200°C, (c) 400°C, (d) 600°C, (e) 800°C and (f) 1,000°C.

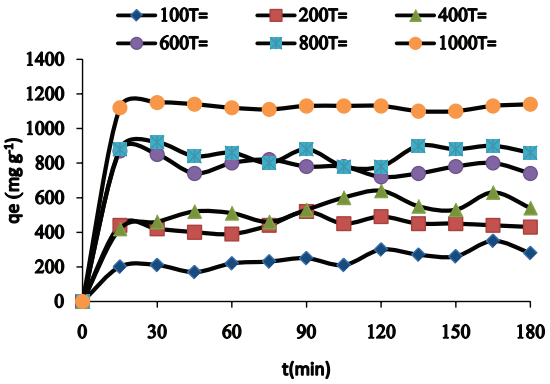

Fig. 5. Effect of contact time for adsorption of BPR onto SD calcinated at different temperatures.

3.2.2. Effect of pH

Solution pH affects adsorption by regulating the adsorbents surface charge as well as degree of ionization of adsorbates present in the solution. Effect of pH on BPR removal by SD is presented in Fig. 6. Adsorption by SD enhanced with the increase in pH from 2 to 6 and thereafter remained nearly constant for pH greater than 6.0. The surface charge may get positively charged, thus making H^+ ions and dye with adsorption on active sites causing a decrease in amount of dye adsorbed. It is observed that q_e of BPR at an initial solution pH 6 was found to be maximum. Therefore, further adsorption experiments were performed at pH > 6. This fact could be, further, described by the pH_{PZC}. For determination of pH_{zpc}, 0.01 M NaCl was prepared and its initial pH was adjusted between 2 and 12 by using HCl or NaOH. Then, 50 mL of NaCl 0.01 M and 0.5 g of SDs were taken in 250 mL Erylenmeyer flasks and were kept for 24 h, then final pH of solutions were measured. The plotted between pH_{final} vs. $pH_{initial}$ was recorded as pH_{pzc}. The pH_{pzc} were found 6.25–7 [36]. The adsorbents with positive surface reacted as

the solution pH < pH_{PZC} and with negative surface reacted as the solution pH > pH_{PZC}. The SDs having pH_{zpc} > 6 exhibited lower adsorption capacity than those with low pH_{zpc} of 2–3. The negative charge density of adsorbent surface improved with further increase in pH, consequently, the dye uptake capacity reduced. This provided strong evidence of electrostatic forces as responsible for BPR adsorption.

3.2.3. Effect of sorbent mass

As the dose of adsorbent can strongly affect the sorption capacity, the adsorption process was done with varied dose of adsorbent (0.001–0.01 g). Such results shown in Fig. 7 indicate that, increasing amount of the adsorbents increases the contact surface area and exchangeable sites, and then increases the percentage of dye removal. After this maximum equilibrium value, the removal efficiency did not increase with increasing adsorbent mass. These results suggest the relationship between adsorbent dosage and removal efficiency is related to the increases in the number of adsorption sites, and that increasing this number had no effect after equilibrium was reached. The decrease in BPR uptake at higher adsorbent dose may be due to competition of the BPR for the sites available [37].

3.3. Adsorption kinetics

Adsorption kinetic studies are significant since not only do they provide valuable insights into the reaction pathways, but also they describe the solute uptake rate which, in turn, controls the residence time of adsorbate at the solid–liquid interface. The experimental data were processed on the basis of two of the most commonly used kinetic models suggested by Lagergren and Ho McKay [38,39]. Lagergren's pseudo-first-order model and Ho's pseudo-second-order model are as Eqs. (3) and (4), respectively:

$$\ln q_t = \ln q_e - k_1 t \quad (3)$$

$$t/q_t = t/q_e + 1/(k_2 q_e^2) \quad (4)$$

In these equations, k_1 is the rate constant of the pseudo-first-order adsorption (min^{-1}), k_2 (g mol^{-1} min) is the rate constant of the pseudo second-order adsorption, q_e and q_t are the amounts of BPR adsorbed on adsorbent (mol g^{-1}) at equilibrium and at time t, respectively. The plotting of ln q_t vs. time (t) for the pseudo-first order kinetic model did not converge well and did not produce straight lines at the studied temperatures.

When the pseudo-second order adsorption equation was applied by plotting (t/q_t) vs. time (t), all the data converged well into a straight line with a high correlation coefficient (R^2). Based on these results, it is clear that the equilibrium adsorption from the pseudo-second order model is much closer to the experimental data as shown in Figs. 8 and 9. The pseudo second order adsorption parameters, the rate constant (k_2), and the amount of BPR adsorbed (q_e) on SDs at equilibrium were calculated from the slope and the intercept. The results are presented in Table 1. A similar phenomenon was observed in modified sawdust of walnut [25]. The latter

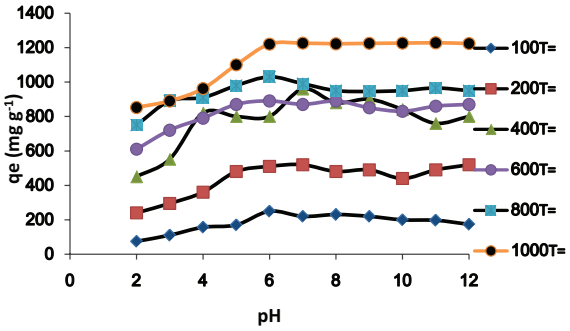

Fig. 6. Effect of pH for adsorption of BPR onto SD calcinated at different temperatures (50 mL BPR 10 mg L^{-1}).

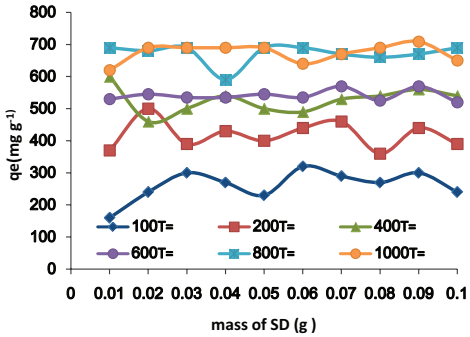

Fig. 7. Effect of sorbent mass for adsorption of BPR onto SD calcinated at different temperatures (50 mL BPR 10 mg L^{-1}).

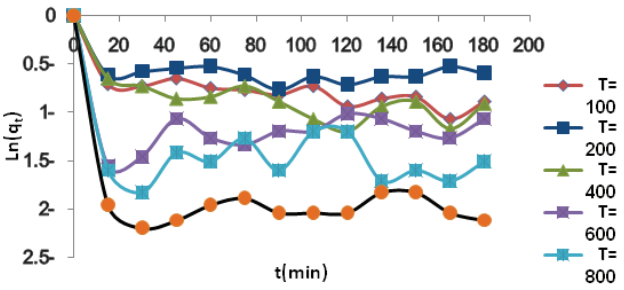

Fig. 8. Pseudo-first order kinetics for adsorption of BPR by SD (50 mL BPR 10 mg L^{-1}).

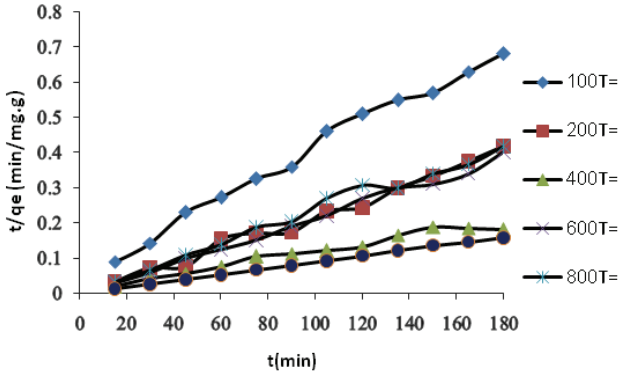

Fig. 9. Pseudo-second order kinetics for adsorption of BPR by SD (50 mL BPR 10 mg L^{-1}).

is based on the assumption that the rate limiting step may be a chemical adsorption involving valance forces through sharing or exchange of electrons between adsorbent and adsorbate.

3.4. Isotherm of adsorption

Adsorption isotherm is basically important to describe how solutes interact with adsorbents, and is critical in optimizing the use of adsorbents. The behavior of SD as an adsorbent was studied by evaluating the equilibrium isotherms.

Adsorption capacity and adsorption behavior of BPR using SD can be illustrated by adsorption isotherm. In this study, adsorption data were fitted by two isotherms namely Freundlich and Langmuir. The Langmuir isotherm is given in Eq. (5) and the Freundlich isotherm is given by Eqs. (6) and (7):

$$C_e/q_e = 1/K_L q_m + C_e/q_m \quad (5)$$

$$Q_e = K_f C_e^{\frac{1}{n}} \quad (6)$$

$$\mathrm{Ln}Q_e = \mathrm{Ln}K_f + \frac{1}{n}\mathrm{Ln}C_e \quad (7)$$

where q_e is the solid phase equilibrium concentration (mg g^{-1}), C_e is the liquid equilibrium concentration of BPR in solution (mg L^{-1}), K_F is the Freundlich constant representing the adsorption capacity (mg g^{-1}), and n is the heterogeneity factor depicting the adsorption intensity, K_L is the equilibrium adsorption constant related to the affinity of binding sites (L mg^{-1}), and q_m is the maximum amount of BPR per unit weight of adsorb bent for complete monolayer coverage (mg g^{-1}).

Results from the Langmuir and Freundlich analysis of the adsorption of BPR on the SD are reported in Table 2. Results from the Freundlich analysis shown in Table 2 indicate that the correlation coefficient is significantly less than the Langmuir analysis in describing the adsorption of BPR. The fact that the Langmuir isotherm fits the experimental data very well may be due to homogenous distribution of active sites on the SD surface.

The values of n indicate the type of adsorption to be favorable (range of 2–10), moderately difficult (in the range of 1–2) or poor adsorption ($n < 1$).

The fundamental properties of the Langmuir isotherm can be explained in terms of dimensionless separation factor R_L:

$$R_L = 1/(1 + k_L C_0) \quad (8)$$

The factor of R_L indicates the type of the isotherm to be unfavorable ($R_L > 1$), favorable ($0 < R_L > 1$), irreversible ($R_L = 0$) and linear adsorption ($R_L = 1$).

3.5. Thermodynamic of adsorption

The equilibrium constant (K_c) is a measure of adsorption which is defined as the ratio of the quantity of the adsorbate retained by the adsorbent to the amount of the adsorbate remaining in solution.

The equilibrium constant was calculated from the following equations, (Eqs. (9)–(11)):

Table 1
Kinetic parameters for adsorption of BPR by SD calcinated at different temperatures (100–1,000°C)

Second order		First order		Calcination temperature of sawdust (°C)
R^2	$K \times 10^{-4}$ (g mg^{-1} min^{-1})	R^2	$K \times 10^{-3}$ (min^{-1})	
0.917	1.65	0.53	3.1	100
0.987	9.98	0.216	1.5	200
0.96	2.08	0.509	3.7	400
0.995	6.76	0.035	1.2	600
0.99	7.118	0.167	3.2	800
0.999	0.27	0.174	4.1	1,000

Table 2
Langmuir and Freundlich constants for the adsorption of BPR by SD calcinated at different temperatures (100–1,000°C)

Langmuir				Freundlich			Calcination temperature (°C) of sawdust
q_m (mg g^{-1})	K_L (l mg^{-1})	R_L	R^2	$K_F \times 10^3$	n	R^2	
10.635	3.35	0.165	0.96	5×10^3	4.61	0.675	100
6.66	2.5	0.209	0.88	7.7×10^4	3.69	0.922	200
13.7	2.44	0.214	0.987	6.6×10^5	5.08	0.741	400
12.82	0.114	1.28	0.97	5.2×10^4	6.33	0.874	600
9.54	1.86	0.263	0.996	1.31×10^5	5.54	0.758	800
11.62	1.62	0.198	0.98	1.5×10^5	6.86	0.698	1,000

$$\Delta G° = -RT \ln K_C \quad (9)$$

$$K_C = C_A/C_S \quad (10)$$

$$\ln K_C = -\Delta G°/RT = -\Delta H°/RT + \Delta S°/R \quad (11)$$

ΔG°, ΔH° and ΔS° are standard Gibb's free energy, enthalpy, and entropy changes, respectively. R is universal gas constant (8.314 J mol K^{-1}), T is absolute temperature (K), K_C (L g^{-1}) is the adsorption equilibrium constant, C_A is the amount of BPR adsorbed on the SD (mg g^{-1}) and C_s is the equilibrium or unadsorbed concentration of the BPR dye in the solution (mg L^{-1}). ΔG° is, in fact, the most fundamental criterion of spontaneity of any reaction. The slope and intercept obtained by the plot of ln K_C against 1/T were used to calculate the ΔH° and ΔS°, respectively. ΔH° and ΔS° were calculated through the slope and intercept of van't Hoff plots of ln K_C vs. 1/T (Fig. 10). Gibbs free energy changes (ΔG°) were, then, calculated from Eq. (11). The results of thermodynamic parameters of BPR adsorption onto SD calcinated at different temperatures (100°C–1,000°C) are given in Table 3.

3.6. Comparison of adsorption parameters of bromophenol dye with different sorbents

Adsorption parameters of different sorbents for phenol dyes were compared and are reported in Table 4. SDs in this study possesses reasonable adsorption capacity in comparison with the other sorbents.

3.7. Regeneration of the spent SD

The adsorption capacity of the $SD_{1,000}$ for BPR after its regeneration has also been studied. The spent SD was regenerated following the process mentioned below. The regenerated samples were again saturated with BPR with the same initial concentration of 50 mg l^{-1}, determining their new adsorption capacity. The physically regeneration of adsorbent was done by heating SD adsorbed BPR at 0°C–400°C. These adsorption- regeneration cycles were carried out 2, 4 and 6 times. The regenerated SD was reused for the adsorption experiment. The temperature of 150°C–200°C is a suitable temperature for regeneration of spent SD. The adsorption capacity of the SD for BPR did not show any significant decrease even after 2 regenerations. After 4 cycles 80% and after 6 cycles 65% of BPR was were removed. The results obtained are depicted in Fig. 11. The value of cycle corresponds to the adsorption capacity of the original SD. Generally, the adsorption capacity of the SD decreases as the number of regeneration cycles increases.

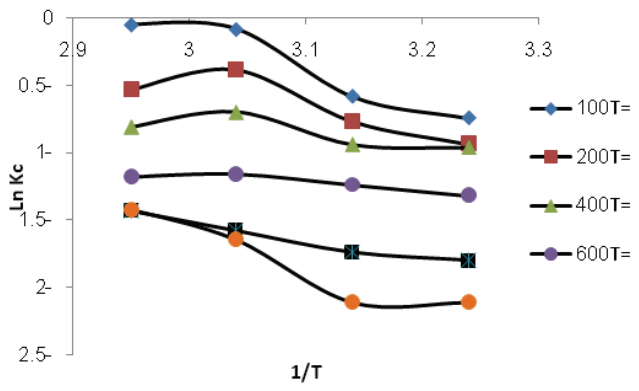

Fig. 10. Ln K vs. 1/T for adsorption of BPR by SD calcinated at different temperatures (100–1,000°C).

Table 3
Thermodynamic parameters of adsorption of BPR by SD calcinated at different temperatures (100–1,000°C)

Calcination temperature (°C)	ΔS° (J mol^{-1} K^{-1})	ΔH° (J mol L^{-1})	ΔG° (KJ mol^{-1})	T (*K*)
100	6.57	2.22	–1.91	308
			–1.54	318
			–2.34	328
			–1.46	338
200	11.55	6.035	–2.46	308
			–2.49	318
			–1.19	328
			–2.28	338
400	37.59	13.918	–2.39	308
			–2.01	318
			–1.049	328
			–1.49	338
600	3.217	4.335	–3.38	308
			–3.27	318
			–3.16	328
			–3.31	338
800	19.995	10.867	–4.04	308
			–4.60	318
			–4.30	328
			–4.018	338
1,000	52.287	21.798	–5.41	308
			–5.59	318
			–4.48	328
			–3.99	338

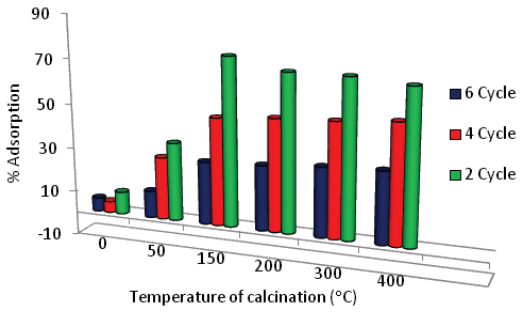

Fig. 11. Effect of physical desorption of BPR onto $SD_{1,000}$.

Table 4
Comparison of adsorption parameters of bromophenol dye with different sorbents (F, Freundlich; L, Langmuir)

Adsorbent	Isotherm model	Kinetic model	q_m (mg g^{-1})	Refs.
Granite	F	1	5.54	[8]
Mesoporous hybrid gel	F	2°	–	[40]
Supported ionic liquids	L	2	–	[41]
Sewage sludge	L	2	26.16	[42]
α-chitin nanoparticles	L	2	4.426	[43]
Silica-filled ENR/PVC	L, F	2°	2.67	[44]
Agricultural waste	–	–	2.67	[45]
Activated carbon	–	–	2.76	[45]
ZnO	L	–	–	[46]
Bentonite carbon composite Bentonite Carbon Composite	F	2	–	[47]
Lignocellulose	L	2	1.454–3.312	[48]
Alumina	F, L	1	0.433	[49]
Activated charcoal	L	2	–	[49]
SD_{600}	L	2	12.8	In his study
$SD_{1,000}$	L	2	11.62	In his study

4. Conclusion

In this paper, the ability of using local adsorbent of SD was studied. The calcination temperature for adsorption of BPR was investigated. The SD sorbents were characterized using SEM and FTIR. Maximum dye was removed within 60 min after the beginning for every experiment. The results showed that as the amount of the adsorbent increased, the percentage of dye removal increased accordingly. Optimum pH value for dye adsorption was determined as >6. The results indicated the sorption of BPR was found to follow pseudo-second-order kinetic model. The thermodynamic constants of adsorption were also evaluated. The negative value of ΔG° confirms the spontaneous nature of adsorption process. Langmuir and Freundlich models were used to analyze the adsorption isotherm. Adsorption behavior was described by a monolayer Langmuir-type isotherm. The maximum BET surface area of $SD_{1,000}$ was 1,050 m^2 g^{-1}. The present investigation showed that SD was a capable low cost adsorbent for removal of BPR from aqueous solutions.

Acknowledgements

We gratefully acknowledge financial support from the Research Council of Islamic Azad University of Yazd.

References

[1] M.F. Siddiqui, Z.A. Wahid, M. Sakinah, Bioremediation and bio fouling perspective of real batik effluent by indigenous bacteria, J. Chem. Environ. Eng., 2 (2011) 302–308.
[2] Y. Anjaneyulu, N. Sreedhara Chary, D. SamuelSuman Raj, Decolourization of industrial effluents – available methods and emerging technologies – A Review, Environ. Sci. Biotechnol., 4 (2005) 245–273.
[3] G. Crini, Non-conventional low-cost adsorbents for dye removal: a review, Bioresour. Technol., 97 (2006) 1061–1085.
[4] S. Hashemian, M. Salimi, Nano composite a potential low cost adsorbent for removal of cyanine, Chem. Eng. J., 188 (2012) 57–63.
[5] U. Singh, R.K. Kumar, Treatment of wastewater with low cost adsorbent–a review, VRSD International J. Tech. Non Tech. Res., 3 (2013) 33–42.
[6] S. Hashemian, A. Foroghimoqhadam, Effect of copper doping on $CoTiO_3$ Ilmenite type nano particles for removal of Congo red from aqueous solution, Chem. Eng. J., 235 (2014) 299–306.
[7] S. Hashemian, A. Dehghanpor, M. Moghahed, $Cu_{0.5}Mn_{0.5}Fe_2O_4$ nanospinels as potential sorbent for adsorption of brilliant green, J. Ind. Eng. Chem., 24 (2015) 308–314.
[8] L.H. Kadhim, Granite as an adsorption surface for the removal of bromo phenol red, bromo cresol green and leishman's stain from aqueous solutions, J. Basrah Res. Sci., 38 (2012) 106–116.
[9] M. Anbia, A. Ghaffari, Removal of malachite green from dye wastewater using mesoporous carbon adsorbent, J. Iran Chem. Soc., 8 (2011) S67–S76.
[10] Y. Uma, C. Sharma, Adsorption kinetics and thermodynamics of malachite green dye unto acid activated low cost carbon, J. Appl. Sci. Environ. Manage., 12 (2008) 43–51.
[11] J. Zhang, Y. Li, C. Zhang, Y. Jing, Adsorption of malachite green from aqueous solution onto carbon prepared from Arundo donax root, J. Hazard. Mater., 150 (2008) 774–782.
[12] M. Hema, S. Arivoli, Adsorption kinetics and thermodynamics of malachite green dye unto acid activated low cost carbon, J. Appl. Sci. Environ. Manage., 12 (2008) 43–51.
[13] M. Nazri Idris, Z. Arifin Ahmad, M. Azmier Ahmad, Adsorption equilibrium of malachite green dye onto rubber seed coat based activated carbon, Int. J. Basic Appl. Sci., 11 (2011) 38–43.
[14] P.S. Syed, Shabudeen, Study of the removal of malachite green from aqueous solution by using solid agricultural waste, Res. J. Chem. Sci., 1 (2011) 88–104.
[15] V.K. Garg, R. Kumar, R. Gupta, Removal of malachite green dye from aqueous solution by adsorption using agro-industry waste: a case study of *Prosopis cineraria,* Dyes Pigments, 62 (2004) 1–10.
[16] B.H. Hameed, Equilibrium and kinetic studies of methyl violet sorption by agricultural waste, J. Hazard. Mater., 154 (2008) 204–212.
[17] S. Hashemian, M. Karimi Ardakani, H. Salehifar, Kinetics and thermodynamics of adsorption methylene blue onto tea waste/$CuFe_2O_4$ composite, Am. J. Anal. Chem., 4 (2013) 1–7.
[18] B.H. Hameed, M.I. El-Khaiary, Kinetics and equilibrium studies of malachite green adsorption on rice straw-derived char, J. Hazard. Mater., 153 (2008) 701–708.
[19] A.A. Ahmad, B.H. Hameed, N. Aziz, Adsorption of direct dye on palm ash: kinetic and equilibrium modeling, J. Hazard. Mater., 141 (2007) 70–76.
[20] P. Pengthamkeerati, T. Satapanajaru, O. Singchan, Sorption of reactive dye from aqueous solution on biomass fly ash, J. Hazard. Mater., 153 (2008) 1149–1156.
[21] M. Hasan, A.L. Ahmad, B.H. Hameed, Adsorption of reactive dye onto crosslinked chitosan/oil palm ash composite beads, Chem. Eng. J., 136 (2008) 164–172.
[22] B.H. Hameed, D.K. Mahmoud, A.L. Ahmad, Sorption of basic dye from aqueous solution by pomelo (*Citrus grandis*) peel in a batch system, Coll. Surf. A: Physicochem. Eng. Asp., 316 (2008) 78–84.
[23] B.H. Hameed, M.I. El-Khaiary, Batch removal of malachite green from aqueous solutions by adsorption on oil palm trunk

fibre: equilibrium isotherms and kinetic studies, J. Hazard. Mater., 154 (2008) 237–244.
[24] J.Y. Farah, N. Sh. El-Gendy, L.A. Farahat, Biosorption of astrazone blue basic dye from an aqueous solution using dried biomass of Baker's yeast, J. Hazard. Mater., 148 (2007) 402–408.
[25] B.H. Hameed, M.I. El-Khaiary, Malachite green adsorption by rattan sawdust: Isotherm, kinetic and mechanism modeling, J. Hazard. Mater., 159 (2008) 574–579.
[26] M. Roosta, M. Ghaedi, A. Daneshfar, R. Sahraei, Removal of malachite green from aqueous solution by zinc oxide nanoparticle loaded on activated carbon: kinetics and isotherm study, J. Indus. Eng. Chem., 20 (2014) 17–28.
[27] M. Jamshidi, M. Ghaedi, K. Dashtian, A.M. Ghaedi, S. Hajati, A. Goudarzi, E. Alipanahpour, Highly efficient simultaneous ultrasonic assisted adsorption of brilliant green and eosin B onto ZnS nanoparticles loaded activated carbon: artificial neural network modeling and central composite design optimization, Spectrom. Chim. Acta Part A: Mol. Biomol. Spectr., 153 (2016) 257–267.
[28] M. Jamshidi, M. Ghaedi, K. Dashtian, S Hajati, A. Bazrafshan, Ultrasound-assisted removal of Al^{3+} ions and Alizarin red S by activated carbon engrafted with Ag nano particles: central composite design and genetic algorithm optimization, RSC Adv., 5 (2015) 59522–59532.
[29] H. Mazaheri, M. Ghaedi, S. Hajati, K. Dashtian, M.K. Purkait, Simultaneous removal of methylene blue and Pb^{2+} ions using ruthenium nanoparticle-loaded activated carbon: response surface methodology, RSC Adv., 5 (2015) 83427–83435.
[30] F. Ferrero, Dye removal by low cost adsorbents: hazelnut shells in comparison with wood sawdust, J. Coll. Interface Sci., 142 (2007) 144–152.
[31] V.K. Garg, R. Gupta, A. BalaYadav, R. Kumar, Dye removal from aqueous solution by adsorption on treated sawdust, Bioresour. Technol., 89 (2003) 121–124.
[32] M.M. Abdel Latif, A.M. Ibrahim, Removal of reactive dye from aqueous solutions by adsorption onto activated carbons prepared from oak sawdust, Desal. Wat. Treat., 20 (2010) 102–113.
[33] J. Shah, M.R. Jan, A. Haq, M. Sadia, Biosorption of cadmium from aqueous solution using mulberry wood sawdust: equilibrium and kinetic studies, Sep. Sci. Technol., 46 (2011) 1631–1637.
[34] J. Shah, M.R. Jan, A. Haq, M. Sadia, Removal of Ni (II) from aqueous solutions using modified carbon derived from Mulberry wood sawdust, J. Chem. Soc. Pak., 34 (2012) 58–66.
[35] J. Shah, M.R. Jan, M. Khan, Removal and solid phase extraction of cadmium from aqueous solutions on magnetic nanoparticle modified sawdust: Kinetics and adsorption isotherm studies, Desal. Wat. Treat., 57 (2016) 9736–9744.
[36] S. Hashemian, K. Salari, Z. Atashi Yazdi, Preparation of activated carbon from agricultural wastes (almond shell and orange peel) for adsorption of 2-pic from aqueous solution, J. Indus. Eng. Chem., 20 (2014) 1892–1900.
[37] S. Saroj, S. Baral, S.N. Dasa, P. Rath, Hexavalent chromium removal from aqueous solution by adsorption on treated sawdust, Biochem. Eng. J., 31 (2006) 216–222.
[38] S. Lagergren, About the theory of so-called adsorption of soluble substances, K. Sven. Vetenskapsakad. Handl., 24 (1898) 1–39.
[39] Y.S. Ho, G. McKay, The kinetics of sorption of basic dyes from aqueous solution by sphagnum moss peat, Can. J. Chem. Eng., 76 (1998) 822–827.
[40] L. You, Z. Wu, T. Kim, K. Lee, Kinetics and thermodynamics of bromophenol blue adsorption by a mesoporous hybrid gel derived from tetra ethoxysilane and bis (trimethoxysilyl) hexane, J. Coll. Interface Sci., 300 (2006) 526–535.
[41] J. Liu, S. Yao, L. Wang, W. Zhu, J. Xu, H. Song, Adsorption of bromophenol blue from aqueous samples by novel supported ionic liquids, J. Chem. Technol. Biotechnol., 89 (2014) 230–238.
[42] S. Bousba, A.H. Meniai, Removal of phenol from water by adsorption onto sewage sludge based adsorbent, Chem. Eng. Trans., 40 (2014) 235–240.
[43] S. Dhananasekaran, R. Palanivel, S. Pappu, Adsorption of methylene blue, bromophenol blue and coomassie brilliant blue by α-chitin nanoparticles, J. Adv. Res., 7 (2016) 113–124.
[44] A.N. Amni, O.R., Abdullah, I. Nazwa, J.B., Azizah, Studies on the adsorption of phenol red dye using silica-filled ENR/PVC beads, J. Emerg. Trends Eng. Appl. Sci., 3 (2012) 845–850.
[45] A.O. Dada, A.A. Inyinbor, A.P. Oluyori, Comparative Adsorption of dyes unto activated carbon prepared from maize stems and sugar cane stems, J. Appl. Chem., 2 (2012) 38–43.
[46] M.S. Mashkour, Decolorization of bromophenol blue Dye under UV- radiation with ZnO as catalyst, Iraqi Natl. J. Chem., 46 (2012) 189–198.
[47] F.M.S.E. El-Dars, H.M. Ibrahim, H.A.B. Farag, M. Zakaria, M.E.H. Shalab, Adsorption kinetics of bromophenol blue and eriochrome black t using bentonite carbon composite material, Int. J. Sci. Eng. Res., 6 (2015) 679–688.
[48] R.M.K. Vala, L. Tichagwa, E.D. Dikio, Evaluation of N-terminated siloxanes grafted onto lignocellulose as adsorbent for the removal of phenol red from water, Int. J. Environ. Sci. Technol., 12 (2015) 2723–2730.
[49] M.J. Iqbal, M.N. Ashiq, Thermodynamics and kinetics of adsorption of dyes from aqueous media onto alumin, J. Chem. Soc. Pak., 32 (2010) 419–428.